The Astrophysical Journal, 848:64 (11pp), 2017 October 10 https://doi.org/10.3847/1538-4357/aa8b74

Assessments of Ali, Dome A, and Summit Camp for mm-wave Observations Using MERRA-2 Reanalysis

Chao-Lin Kuo[1,2]
[1] Department of Physics, Stanford University, Stanford, CA 94305, USA
[2] Kavli Institute for Particle Astrophysics and Cosmology, SLAC National Accelerator Laboratory, 2575 Sand Hill Road, Menlo Park, CA 94025, USA
Received 2017 August 3; revised 2017 September 7; accepted 2017 September 7; published 2017 October 12

Abstract

NASA's latest MERRA-2 reanalysis of the modern satellite measurements has made atmospheric data easily accessible with unprecedented uniformity, fidelity, and completeness. In this paper, these data are used to evaluate five sites for millimeter-wave (mm-wave) observations. These include two established sites (South Pole and Chajnantor, Atacama), and three new sites (Ali in Tibet, Dome A in Antarctica, and Summit Camp in Greenland). Atmospheric properties including precipitable water vapor (PWV), sky brightness temperature fluctuations, and ice and liquid water paths are derived and compared. Dome A emerges to be the best among those evaluated, with PWV and fluctuations smaller than the second-best site, South Pole, by more than a factor of 2. It is found that the higher site in Ali (6100 m) is on par with Cerro Chajnantor (5612 m) in terms of transmission and stability. The lower site in Ali (5250 m) planned for the first stage of observations at 90/150 GHz provides conditions comparable to those on the Chajnantor Plateau. These analyses confirm Ali to be an excellent mm-wave site in the Northern Hemisphere that will complement well-established Southern sites. According to MERRA-2 data, the observing conditions at Summit Camp are also comparable to Cerro Chajnantor. However, it is more affected by the presence of liquid water clouds.

Key words: atmospheric effects – cosmic background radiation – cosmology: observations – gravitational waves – radiative transfer – site testing

1. Introduction

Searching for imprints of primordial gravitational waves using CMB polarization (Seljak & Zaldarriaga 1997) and probing the event horizon of black holes using very long-baseline interferometry (VLBI; Ricarte & Dexter 2015) are two of the most exciting topics in modern astrophysics. These two endeavors share similar scientific themes in that CMB polarization probes the beginning of time, and VLBI such as that performed by the Event Horizon Telescope (EHT) studies the edge of space. Experimentally, scientists working in these two areas must make sensitive measurements through the atmosphere in the handful of millimeter-wave (mm-wave) frequency bands. In these atmospheric "windows," the opacity depends strongly on observing conditions, particularly the integrated humidity. The most notable mm-wave atmospheric windows (3, 2, 1.4, and 1.1 mm; or 90, 150, 220, and 280 GHz) near the peak of the CMB radiation can be rendered opaque if the precipitable water vapor (PWV) is larger than a few mm. Not only do water vapor and atmospheric column density introduce attenuation in the astronomical signal, Kirchhoff's law of thermal radiation demands that the emission from the intervening media, and therefore the thermal background against which the measurements are made, is proportional to the product of the optical depth and the physical temperature (>200 K). This latter effect makes it desirable to observe at sites with the lowest possible opacity in the mm-wave windows, even when the attenuation of the signal starts to become a secondary factor when the transmission is larger than 90%.

In addition to adding a constant background, the concentration of water—the most important mm-wave absorber in the atmosphere—tends to fluctuate because the saturated water vapor pressure depends strongly on the temperature. As a result, the distribution of water in different phases greatly amplifies the density fluctuations in the dry air. Vapor-induced fluctuations in optical depth create brightness temperature fluctuations in CMB measurements and introduce phase errors in long-baseline interferometry.

So far, ground-based CMB measurements have been made most successfully at the South Pole and the Atacama Desert. EHT has also gathered data from both sites. In addition to the science data collected, the observing conditions at these sites have been characterized over the last few decades using a variety of techniques, including coherent radiometers with frequencies tuned to the wings of the water lines, far-infrared (IR) continuum photometers, and radiosonde launches that collect temperature, humidity, and pressure data twice a day.

Dome A, the highest point of the Antarctic Plateau (4093 m), is known to be another site with great potential. The latest Fourier Transform Spectrometer (FTS) data showed that it is possibly the best submm/THz site on Earth (Shi et al. 2016). Recently, the CMB and VLBI communities also became interested in exploring other sites to seek either larger sky area or more complete *uv* coverage.[3] Science with CMB lensing especially benefits from large sky coverage that includes a northern site (Wu et al. 2014; CMB-S4 Collaboration 2016). Summit Camp, Greenland and Ali, Tibet have been proposed as candidate locations in the Northern Hemisphere for such observations.

Efforts are being made to directly characterize three sites using various instruments. In this paper, the MERRA-2 reanalysis (Bosilovich et al. 2015) produced by NASA's Global Modeling and Assimilation Office (GMAO) has been used to evaluate these sites. While on-site radiometer measurements are not to be replaced by the "armchair" approach

[3] http://www.cfa.harvard.edu/greenland12m

described in this paper, the most recent MERRA-2 data products derived from IR through microwaves provide unparalleled completeness and uniformity of the atmospheric properties, making it very straightforward to evaluate different sites on an equal footing. In this paper, MERRA-2 analysis products have been used to derive PWV measurements with intervals as short as 1 hr. These results are found to be in good agreement with prior measurements at the South Pole and Atacama. The same analyses are carried out for Ali, Summit Camp, and Dome A.

This paper outlines a recipe to use the MERRA-2 data products to comprehensively evaluate candidate sites. Dome A is confirmed to be the premier mm/submm site on Earth, with exceedingly low PWV and brightness temperature fluctuations all year around. The proposed Northern Hemispheric sites Ali, Tibet and Summit Camp, Greenland are comparable to Atacama, although both sites are noticeably cloudier. Before this paper, weather data from CFSR were used to evaluate the Ali site (Ye et al. 2016). Although the results in that work show the initial promise of Ali, they are limited by a combination of poor grid resolution and a lack of altitude information. Data taken from a remotely operated 220 GHz tau-meter have been reported for the Summit Camp by the ASIAA (Institute of Astronomy and Astrophysics, Academia Sinica) group (Matsushita et al. 2017). Dome A has recently been characterized with an FTSinstalled by the Purple Mountain Observatory (PMO) and Harvard-Smithsonian Center for Astrophysics (CfA; Shi et al. 2016). The results presented in this paper are in excellent agreement with these heroic efforts, but with more emphasis on long integrations such as CMB and other deep-field mm-wave measurements. To the author's knowledge, this is the first time the effects of clouds, quantified by IWP (ice water path) and LWP (liquid water path), have been systematically assessed for mm-wave observations. Finally, this paper presents the first comprehensive comparisons of brightness temperature fluctuations between Dome A, South Pole, Atacama, Ali, and Summit Camp using a uniform methodology.

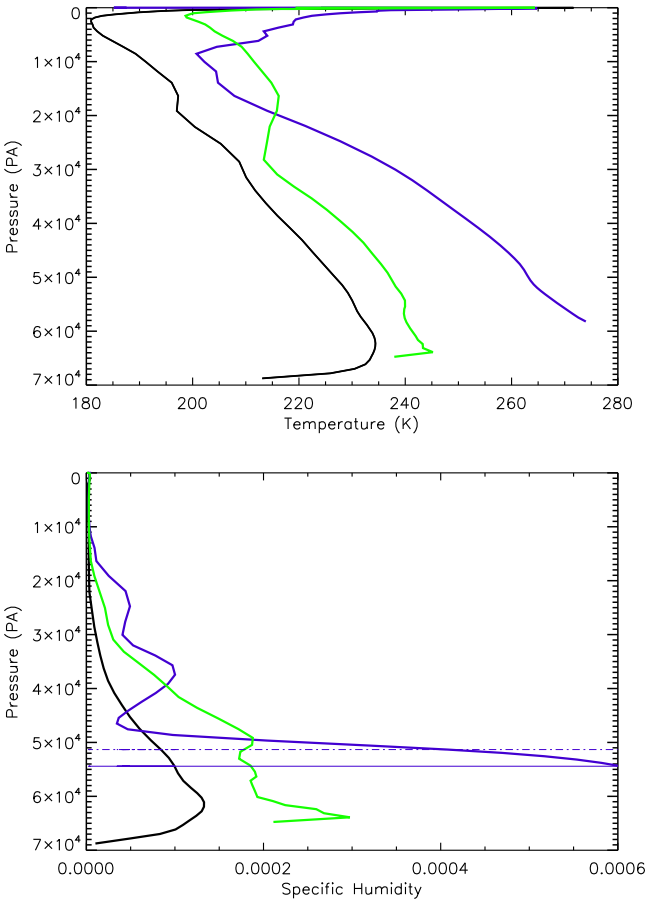

Figure 1. Example wintertime temperature (top) and humidity (bottom) profiles from MERRA-2 reanalysis. The three lines are for the South Pole (black), Summit Camp, Greenland (green), and Chajnantor (blue). The strong Antarctic surface inversion is clearly resolved in both temperature and humidity. The horizontal lines mark the approximate elevations of Simons Observatory (top) and Cerro Chajnantor (bottom).

2. Data and Analysis

The Modern-Era Retrospective Analysis for Research and Applications, Version 2 (MERRA-2) is the latest atmospheric reanalysis of the modern satellite era initiated by NASA's GMAO. It uses state-of-the-art processing of observations from the continually evolving global observing system that employs an array of instruments from near-IR to microwaves (McCarty et al. 2016). The redundantly observed atmospheric quantities have been forced to obey the equation of continuity and other hydrodynamical relations using large-scale numerical modeling. Data taken from different instruments, or retrieved with different methodologies, have been extensively compared and calibrated. MERRA-2 data are also made to be consistent with other atmospheric data such as radiosonde launches when they are available. Altogether, this data set offers reliable measurements of basic meteorological fields such as temperature, pressure, specific humidity, ice/liquid cloud fraction, and wind speed/direction in three dimensions, as well as other atmospheric quantities (CO_2, O_3, aerosol) that are more relevant to astronomers than to astronomy.

Several MERRA-2 products provide sufficient pressure resolution to map the low tropospheric profiles, easily resolving the Antarctic inversion layer in both temperature and specific humidity (Figure 1). Previous MERRA products lack the resolution to reliably calculate PWVs (Shi et al. 2016).

As mentioned earlier, PWV distribution is the most important measure for site quality. But MERRA-2 offers a lot more information that is also important for mm-wave observations. For example, the presence of ice and liquid clouds can impact CMB observations that rely on relentless integrations with high-observing duty cycles, but is often overlooked in conventional site surveys focusing on opportunistic VLBI or THz spectroscopy of bright sources. MERRA-2 provides measurements of IWPs and LWPs, which, when measured in kg m^{-2}, are equivalent to the same molecular column density for mm of PWVs in solid and liquid phases. Through analyses of MERRA-2 data, the impacts of clouds—particularly clouds consisting of supercooled liquid droplets—on CMB observations for these sites are evaluated.

MERRA-2 published many analysis products for different applications in atmospheric modeling and climate monitoring. All the results in this paper are derived from four data products: (1) 3D three-hour interval, time-averaged meteorological fields with 72 model pressure levels (M2T3NVASM.5.12.4), e.g., Figure 1; (2) same as the above, but for instantaneous quantities (M2I3NVASM.5.12.4); (3) 2D integrated diagnostic meteorological fields with 1 hr time intervals, time-averaged (M2T1NXSLV.5.12.4); (4) same as the above for instantaneous quantities (M2I1NXASM.5.12.4). All four data products

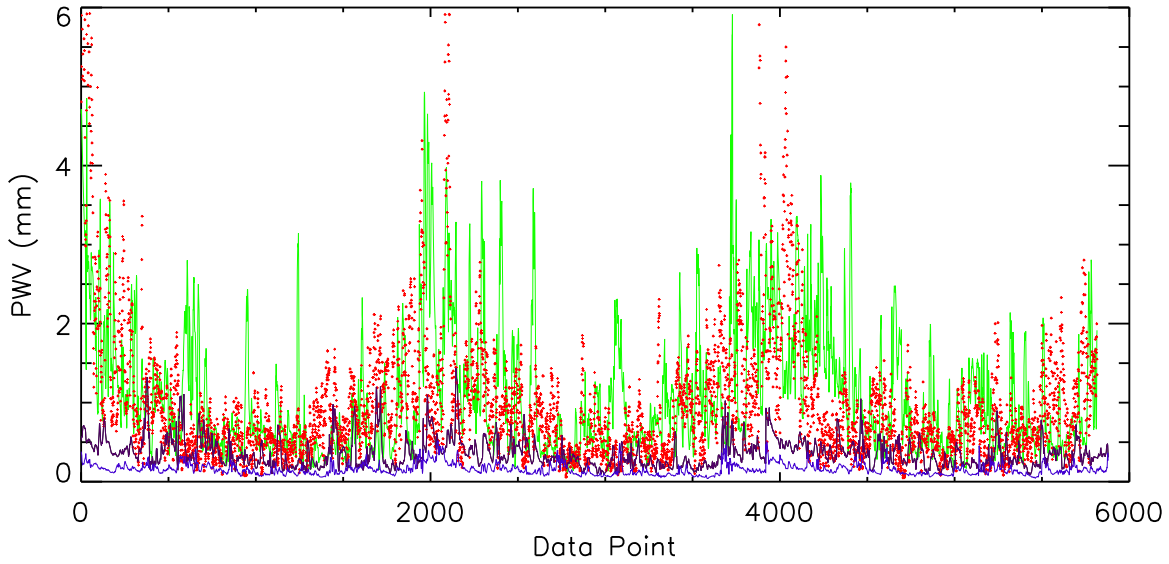

Figure 2. Calculated PWVs for South Pole (black), Dome A (blue), Greenland (green), and Ali2 (red dots). The four summer months have been excluded for all these sites. The data are otherwise continuous without any gaps, 3 hr per point.

come with a grid resolution of $0.^{\circ}65 \times 0.^{\circ}5$ in (longitude, latitude).

The data products with finer pressure resolution ((1) and (2)) are chosen to capture the temperature and humidity near the surface, especially for the Antarctic sites. However, since the spatial resolution of MERRA-2 is insufficient to resolve individual peaks for siting observatories, the altitude data in (1) and (2) are used to evaluate potential sites at different elevations. This is done under the assumption (the "elevation hypothesis") that the variations within a MERRA-2 grid are mostly due to the elevation, at least on average. Specifically, the PWV on a mountaintop within the grid point has been calculated as the integral of specific humidity starting at the altitude (pressure) of the candidate site. As discussed in Section 4, PWVs calculated using this method are consistent with prior data taken at Cerro Chajnantor and Simons Observatory, two sites located within the same grid point but at different elevations. The same assumptions are made in evaluating candidate sites within the Ali grid point, at 5250 m (Ali1) and 6100 m (Ali2). For South Pole, Dome A, and Summit Camp, the ground elevation does not vary significantly within a MERRA-2 grid point.

The PWV can be calculated as the integral of specific humidity q as a function of pressure p:

$$\mathrm{PWV} = \frac{1}{\rho g}\int_{p_0}^{0} q dp, \tag{1}$$

where p_0 is the pressure at the elevation. Figure 2 shows examples of calculated PWVs.

Brightness temperature fluctuations introduce phase noise in VLBI and $1/f$ noise in polarization data in scanning/differencing CMB experiments (when relative gain error is present). While the spatial resolution of MERRA-2 (~50 km) is insufficient to directly infer sky temperature fluctuations on angular scales that are relevant to astronomical measurements, the richness of MERRA-2 data products offers several ways to estimate brightness temperature fluctuations for these purposes.

MERRA-2 3D data are provided at 3-hr intervals. Variance of inferred PWVs provides information on the sky brightness variations (and phase stability) longer than this timescale. On the other hand, differencing the 3D instantaneous and time-averaged specific humidity (q_i and q_a) provides a measurement of instantaneous spatial variations with characteristic scales of a few hundred meters (Figure 3). Since these scales are still within the 3D regime of Kolmogorov–Taylor turbulence, the same fluctuations should appear as the angular brightness temperature variations across the sky. This method is analogous to using redshift information to map the large-scale structure. Specifically, fluctuations on scales of 200 m appear as $\sim 10^{\circ}$ (multipole $\ell \sim 20$) angular variations, which are very relevant to measurements of primordial B-modes. The amplitude of the fluctuations defined this way is given by

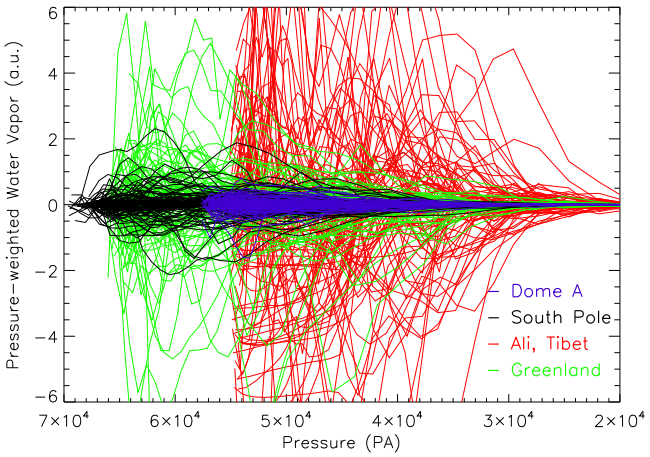

Figure 3. Spatial fluctuations of water vapor measured by MERRA-2. Fluctuations on scales of a few hundred meters seen in this plot are used to derive dPWV for site evaluation.

$$d\mathrm{PWV} \equiv \frac{1}{\rho g}\left[\int_{p_0}^{0} (q_i - q_a)^2 p dp\right]^{1/2}. \tag{2}$$

The corresponding brightness temperature fluctuations at each frequency are calculated by the radiative transfer code *am* (Paine 2017).

This paper also uses another method to reveal short-timescale fluctuations. For the 2D data with 1-hr intervals,

MERRA-2 supplies both the instantaneous and time-averaged data. Because the instantaneous data contain aliased noise but the time-averaged data do not, differencing these data provides measurements of temporal variations taking place shorter than two hours, e.g., for PWVs and LWPs (denoted by ΔPWV, ΔLWP, respectively). This is especially useful for the South Pole and Summit Camp, where the 2D data are directly applicable due to the flat terrain.

It should also be noted that temporal variations are closely related to angular brightness variations in the screen model of the atmospheric fluctuations, in which the large-scale wind carries a "screen" of spatially varying distribution of water vapor and droplets (Lay & Halverson 2000; Bussmann et al. 2005). In the past, this model successfully described the behavior of brightness temperature fluctuations and phase noise at mm-waves. For a wind speed of 2 m s^{-1} and screen height of 1 km, 30-minute-long temporal variations correspond to brightness fluctuations on the largest angular scales observable (∼90°), or multipole $\ell \sim 5$.

While d and Δ quantities are not designed to precisely describe the angular power spectra, they should be good proxies for angular fluctuations of brightness temperature relevant for CMB observations. These analyses could provide reliable comparison of brightness temperature fluctuations for different sites, which is the main purpose of this paper and other similar endeavors.

3. Impact on Observations

Water is a powerful absorber at mm/submm wavelengths. While water vapor makes up a small fraction of the atmosphere, PWV is the most important quantity that characterizes the quality of the site for mm-wave and submm observations. At frequencies higher than 150 GHz, observations are only effective when PWV drops below 1 mm. Since superconducting transition edge sensors (TES) have become standard CMB detectors, reliable measurements of PWV distribution became even more important, because TES can only operate under optical loading up to a certain saturation power, above which the responsivity of TES drops rapidly. A full distribution (histograms) of PWV can be used to tune the thermal conductance (G) and critical temperature (T_c) to optimize the sensitivity of the experiment over extended period of integration. Without such information, conservative parameters that degrade sensitivity are often chosen to avoid detector saturation.

Compared to water vapor, non-precipitating ice/liquid water (i.e., clouds) makes up an even smaller mass fraction. Liquid droplets and ice crystals back-scatter thermal radiation from Earth's warm surface into the line of sight of the telescope, increasing the observed brightness temperature. Because of their extended shapes, ice crystals scatter strongly in the submm and far-IR. At mm-wave and microwave wavelengths where the Rayleigh approximation holds, liquid droplets scatter more strongly than ice crystals because of the higher index of refraction. For the same molecular column density, liquid water is much more emissive than vapor or ice. Therefore, even very thin liquid water clouds are very detrimental to mm-wave observations (Figure 4). Unfortunately, supercooled liquid clouds exist way below "freezing," down to a temperature of ∼228 K. Based on the MERRA-2 data, LWPs often coexist with IWPs and start to impact mm-wave brightness temperature when PWVs are greater than about 0.5 mm, especially for Ali and Summit Camp. The effects of IWPs (cirrus clouds) are found to be small for all the sites considered in this paper.

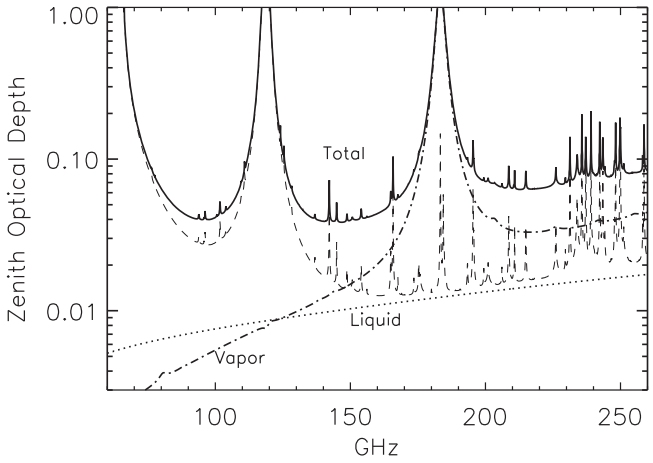

Figure 4. *Am* spectra for the dry and wet components of the atmosphere (PWV = 0.65 mm, LWP = 0.01 kg m^{-2}).

MERRA-2 data have been used by Paine (2017) to derive the mean temperature, humidity, and ozone profiles as the inputs to radiative transfer calculations (*am*) for different sites, including the ones considered here. In this paper, each set of meteorological measurements has been directly used for an *am* calculation. While this requires many more calls, the brightness temperature (T_b) distribution obtained this way explicitly includes all the correlations between pressure levels and across different quantities (such as temperature, humidity, and clouds). For CMB, sky temperature fluctuations do not fundamentally impact the polarization measurements. If the fluctuations are unpolarized, they can be reduced by better gain-fitting, or by rapid modulations of polarization by a half-wave-plate. But at present, brightness temperature fluctuations on timescales longer than a few seconds still impose a practical limitation on science grade CMB polarization measurements. Results from the fluctuation analysis presented in this paper should be very useful for future planning, such as the CMB-S4 effort (Abazajian et al. 2015; CMB-S4 Collaboration 2016).

Atmospheric fluctuations in polarization can be generated by patches of ice crystals descending through air, or aligned by varying wind. Such polarization fluctuations are an irreducible source of noise, because they cannot be mitigated by either method mentioned above. While MERRA-2 data provide measurements of IWP, no attempts are made in this paper to estimate the degree of polarization of the scattered ground radiation, which depends on the shapes and sizes of the crystals and the degree of alignment. Such analysis is better done as an empirical cross-correlation between mm-wave polarization signal and IWP, and is beyond the scope of this paper.

Although liquid droplets are spherical, they can scatter an anisotropic radiation field (specifically, the quadrupole moment) into the line of sight with a small amount of polarization. This process is analogous to the generation of E-mode polarization at the surface of last scattering (Rees 1968). Since the large-scale radiation field experienced by water molecules ($T = T_{sky}$ for $\theta < \pi/2$; $T = T_{gnd}$ for $\theta > \pi/2$) lacks any quadrupole moments, the typical amplitude of the quadrupole moment is at the 10s of mK level, which leads to negligible level of polarized noise.

Finally, it should be noted that dry air has a significant contribution to opacity at 90 GHz, a quintessential CMB

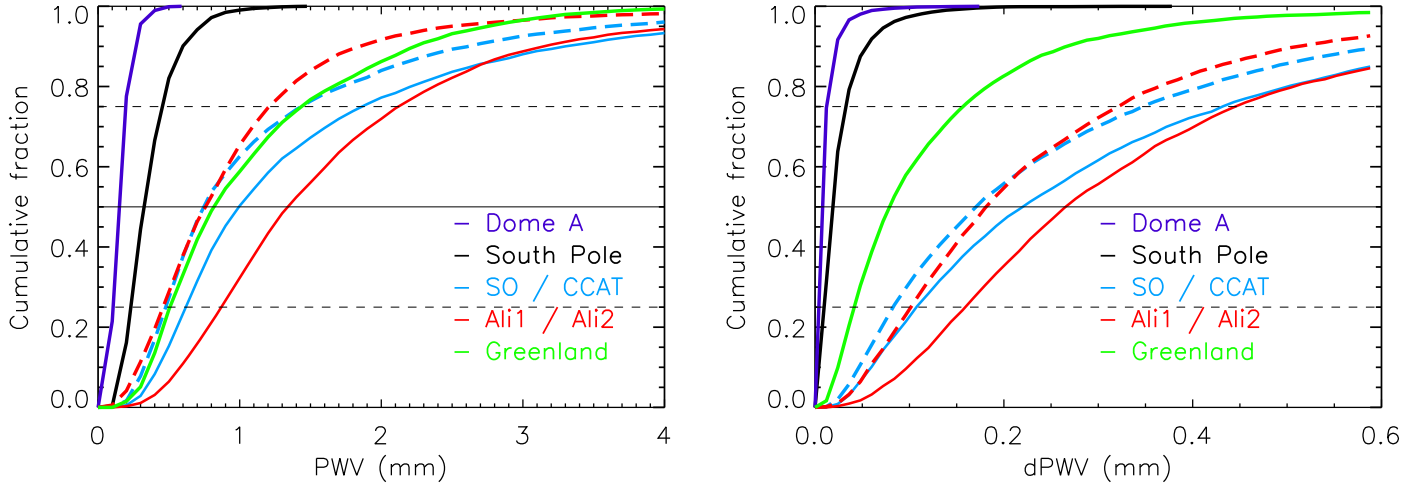

Figure 5. (Left) the cumulative distribution of precipitable water vapor for Dome A, South Pole, Chajnantor (SO/CCAT), Ali1/Ali2, and Summit Camp, Greenland. For Chajnantor and Ali, two sets of curves are given for lower (solid) and higher (dashed) sites. Greenland and Ali2 both provide observing conditions similar to those of Cerro Chajnantor. (Right) the cumulative distribution of *d*PWV, the fluctuation measure defined in Equation (2). Dome A and South Pole are superb for both their low PWV quartiles and high stability. Table 1 provides a numerical summary of Figure 5.

channel, because of proximity to a strong oxygen line. Observations made in this window are particularly advantageous at higher mid-latitude sites (Ali and Atacama), somewhat compensating for their higher PWVs compared to the Antarctic sites.

4. Results

In this section, results from the MERRA-2 analyses, including the PWVs, IWPs, LWPs, T_b, and their fluctuations are presented, first for Atacama and South Pole as a validation, and then for the proposed sites. The data are taken from three years of MERRA-2 reanalysis (2014–2016), excluding summer months (May–August for the Northern Hemisphere and November–February for the Southern Hemisphere).

4.1. AERRA-2 Properties of The Established Sites

Atacama Desert. The Atacama Cosmology Telescope (ACT)[4] and POLARBEAR Telescope[5] (jointly the Simons Observatory, SO) are located at an elevation of 5,190 m in Cerro Toco, about 200 m higher than the Chajnantor Plateau, where ALMA (Atacama Large Millimeter Array) is located. Higher than the SO site is Cerro Chajnantor (5612 m), the location selected for CCAT-prime[6] and TAO.[7]

Because of these prominent projects, the Atacama Desert has been extensively characterized by various radiometers and far-IR tau-meters. The lower and higher sites are located within the same MERRA-2 grid and can be used to validate the elevation hypothesis: setting the starting point of the integral in Equation (1) to be the ground pressure of the site.

Extensive site surveys of the Chajnantor area have been carried out for ALMA.[8] Additionally, in a series of papers spanning more than a decade, Radford & Peterson reported distributions of PWV inferred by 350 μm continuum measurements carried out at Maunakea, Chajnantor, and the South Pole (Peterson et al. 2003; Radford 2012; Radford & Peterson 2016).

The PWV distributions derived from MERRA-2 for SO and Cerro Chajnantor (Figure 5; Table 1) are comparable with these archival measurements, although the PWV derived from the 350 μm tipper measurements for Cerro Chajnantor are noticeably lower than MERRA-2 (0.66 versus 0.75 mm) (Radford 2012). It is not clear whether the difference is simply due to yearly variations or conversions from opacity to PWV. On the other hand, the APEX (5104 m) 183 GHz water line data are in very good agreement with the MERRA-2 values for SO (median of 0.99 versus 1.1 mm).

The PWV scale-height derived from MERRA-2 (1475 m at the median) agrees well with Cortes et al. (2016), who reported an exponential scale-height of 1379 m at the median using two identical radiometers, which was somewhat larger than the value given by Radford & Peterson (2016) of 1080 m.

South Pole. The geographical South Pole (elev. 2835 m) has been home to a series of successful CMB experiments since the 1990s. The US National Science Foundation provided excellent logistic support to the South Pole-based experiments. Currently, the BICEP3 telescope (Wu 2016), Keck Array (Kernasovsky et al. 2012), and the 10 m South Pole Telescope[9] are observing from the South Pole at mm-wave bands.

The observing conditions at the South Pole have been extensively characterized (Peterson et al. 2003; Yang et al. 2010; Chamberlin & Crossman 2012; Radford & Peterson 2016). The dry, calm, and extremely cold conditions prevalent on the Antarctic Plateau allow it to surpass the higher Chajnantor in mm/submm atmospheric transparency. The PWV distributions derived from the MERRA-2 reanalysis are presented in Figure 5 and Table 1. The 2014–2016 8-month PWV quartiles of 0.231/ 0.321/0.448 mm affirm South Pole's tremendous advantage for uninterrupted mm-wave observations. These numbers are in excellent agreement with those reported elsewhere, e.g., in reference Yang et al. (2010), which estimated the best quartile and median PWV to be 0.23 and 0.32 mm. In Table 1, the median values are shown in bold for clarity.

[4] act.princeton.edu
[5] bolo.berkeley.edu/polarbear
[6] http://www.ccatobservatory.org
[7] http://www.ioa.s.u-tokyo.ac.jp/TAO/en
[8] ALMA memos, 187, 382, 512, 521.
[9] pole.uchicago.edu/spt

Table 1
Comparisons between mm/submm Sites

	elev.(m)	PWV(mm)			*d*PWV (mm)			IWP (kg m^{-2})			LWP (kg m^{-2})		
		25%	50%	75%	25%	50%	75%	25%	50%	75%	25%	50%	75%
Dome A	4093	0.105	**0.141**	0.191	3.65E-03	**6.56E-03**	1.21E-02	8.09E-05	**2.30E-04**	6.11E-04	…	…	…
South Pole	2835	0.231	**0.321**	0.448	1.04E-02	**1.77E-02**	3.17E-02	1.96E-04	**1.14E-03**	3.97E-03	…	**1.77E-05**	4.54E-04
Chajnantor (SO)	5,190	0.618	**0.993**	1.871	1.07E-01	**2.20E-01**	4.32E-01	…	**2.23E-05**	1.69E-03	…	…	4.33E-05
Cerro Chajnantor	5612	0.48	**0.746**	1.439	8.28E-02	**1.71E-01**	3.47E-01	…	**2.15E-05**	1.69E-03	…	…	3.22E-05
Ali1	5250	0.871	**1.343**	2.125	1.59E-01	**2.66E-01**	4.45E-01	7.62E-06	**1.16E-03**	1.14E-02	…	**8.70E-04**	8.91E-03
Ali2	6100	0.459	**0.759**	1.207	1.01E-01	**1.81E-01**	3.21E-01	1.70E-06	**9.91E-04**	1.08E-02	…	**5.36E-04**	7.56E-03
Greenland	3216	0.509	**0.817**	1.436	4.14E-02	**7.89E-02**	1.56E-01	6.34E-04	**2.54E-03**	8.34E-03	5.18E-04	**3.57E-03**	1.15E-02

Note. The median values are shown in bold for clarity.

Besides its low PWV, it has been established that the South Pole atmosphere is extremely stable, with low sky temperature fluctuations due to a lack of diurnal variations and its location away from the oceans (Peterson et al. 2003). It has been shown that the supreme stability of the sky brightness temperature at the South Pole truly separates it from Chajnantor and other mid-latitude sites such as Maunakea (Lay & Halverson 2000; Bussmann et al. 2005; Sayers et al. 2010; Errard et al. 2015). These direct observations of spatial fluctuations agree well with the simple but uniform fluctuation measures proposed in this paper (Sections 2 and 4.4).

4.2. Basic Properties of the Candidate Sites

Dome A (Kunlun Station). Dome Argus (4093 m) is located at the highest point of the Antarctic Plateau, 1260 m higher than the South Pole and further inland. Since the early 2000's, Australian, Chinese, and US groups have identified Dome A as a potentially game-changing site for THz astronomy. This assessment was initially supported by weather data and some limited on-site measurements during the summer. The Chinese Kunlun Station was established at Dome A in 2009, four years after it was visited for the first time. Ever since, tremendous efforts have been made to characterize its THz transmittance in the winter, when temperatures and submillimeter opacities are at their lowest. A Schottky Diode-based receiver was online for 204 days in 2008 to measure sky opacity at 661 GHz (Yang et al. 2010). The inferred best quartile and median PWV are 0.1 and 0.14 mm, which are in good agreement with the MERRA-2 results presented in this paper (0.105, 0.141 mm). Recently, 19 months of FTS data covering 0.75–15 THz were analyzed, revealing the THz windows promised by the low PWV (Shi et al. 2016).

In this paper, it is shown that the PWV quartiles at Dome A are more than a factor of two smaller than those of the South Pole, using data retrieved by the same satellite-borne instruments and using the same analysis method. The implication is that in addition to being a premier THz site, Dome A is superior to the South Pole for long CMB integrations at high frequencies. For example, the 3rd-quartile 220 GHz sky brightness temperature is 30% lower at Dome A than at the South Pole.

Furthermore, the quartile values for *d*PWV (fluctuations as defined in Section 2), IWPs (cirrus clouds), and LWPs (liquid clouds) are all much lower at Dome A than they are at the South Pole (Figure 5 and Table 1). These will be discussed further in Sections 4.3 and 4.4

Summit Camp, Greenland. Summit Camp is located at an elevation of 3216 m in Greenland, 300–500 km inland. The current research areas at the station include atmospheric sciences, cosmic rays, and neutrino physics. CfA and ASIAA are collaborating on a major project that will install a 12 m submm antenna (GLT, Greenland Telescope[10]) for VLBI studies of the supermassive black hole at the center of M87. Summit Camp is also a potential Northern Hemisphere site for the next stage of CMB programs. The extreme polar environment and lack of diurnal variations could in principle provide uninterrupted observing conditions similar to the South Pole. Its latitude of 72°.5 N makes it possible to form "cross-linked" measurements of the sky. However, continuous operation of CMB telescopes requires major improvements to the infrastructure and logistic support that are much beyond the level of GLT, which will only be online for 10% of the time.

The ASIAA team deployed a radiometer manufactured by Radiometer Physics GmbH (RPG) to monitor zenith 220 GHz opacity over the past few seasons. They reported that the inferred PWV is about 10% larger than those derived from their own MERRA-2 analyses. The measured PWV median of 0.79 mm for the 6 winter months over the last 3.5 years (Matsushita et al. 2017) is in good agreement with the results reported in this paper, which put the PWV quartiles at 0.509/0.817/1.436 mm. The quartile range is comparable to Cerro Chajnantor and Ali2 considered below (Figure 5; Table 1). However, MERRA-2 data indicate that liquid water is present at a surprisingly high level in Greenland. LWP and its fluctuations can significantly affect the efficiency of long integrations but are often overlooked in the literature (more discussions in Sections 4.3 and 4.4).

Ali, Tibet. Ali is the site of a major Chinese initiative on CMB and primordial gravitational waves. Located on the dry side of the Himalayas at the latitude of 32° N, the site has access to a large portion of the sky, especially the Galactic northern hole, which is difficult to observe from Atacama because the field is available from the Southern Hemisphere often when the weather is less than ideal. Ali is easily accessed through daily commercial flights from Lhasa, Tibet's capital city. Ample electricity is available through the city grid, eliminating the need for generators on-site and the logistic challenges of maintenance and transportation of diesel fuel. Furthermore, the site is about one hour from a major town of 20,000 people, Shiquanhe, where food and other supplies are available throughout the year. The town is still under fast development so construction services and equipment are easily obtained in the area.

The MERRA-2-derived PWV for Ali has been checked against radiosonde launches by the local weather station for the period between 2016 October–November. The two data sets showed excellent agreements (Li et al. 2017). From MERRA-2 data, it is confirmed that Ali1 (5250 m), the site planned for the first 90/150 GHz telescope, is a very decent mm-wave observing site, with PWV quartiles coming in at 0.871/1.343/2.125 mm between September and April. Although the median PWV is somewhat larger than that of SO (0.993 mm), the 85% cumulative PWV value is nearly the same as that of the SO. Since the four worst summer months are already excluded, this is perhaps a more representative comparison for high-duty cycle observations such as CMB.

In Figure 5 and Table 1, the properties for Ali2, a proposed site at 6100 m within the same MERRA-2 grid, are also presented. The inferred PWV quartiles (0.459/0.759/1.207 mm) are very similar to Cerro Chajnantor and Summit Camp, Greenland. The derived PWV scale-height for the Ali area is 1490 m at the median. The level of LWP is found to be higher in Ali than in Atacama, though not as high as Summit Camp. The Ali2 observatory, when established, will be a premier mm/submm site at the mid-latitude in the Northern Hemisphere.

4.3. Impact of Ice and Liquid Clouds

As discussed earlier, MERRA-2 retrieves PWVs, LWPs, and IWPs separately using measurements over a wide frequency range. In Figure 4, optical depth due to various components of the atmosphere is shown for representative values of PWV (0.64 mm) and LWP (0.01 kg m^{-2}) in winter at the Summit

[10] http://www.cfa.harvard.edu/greenland12m

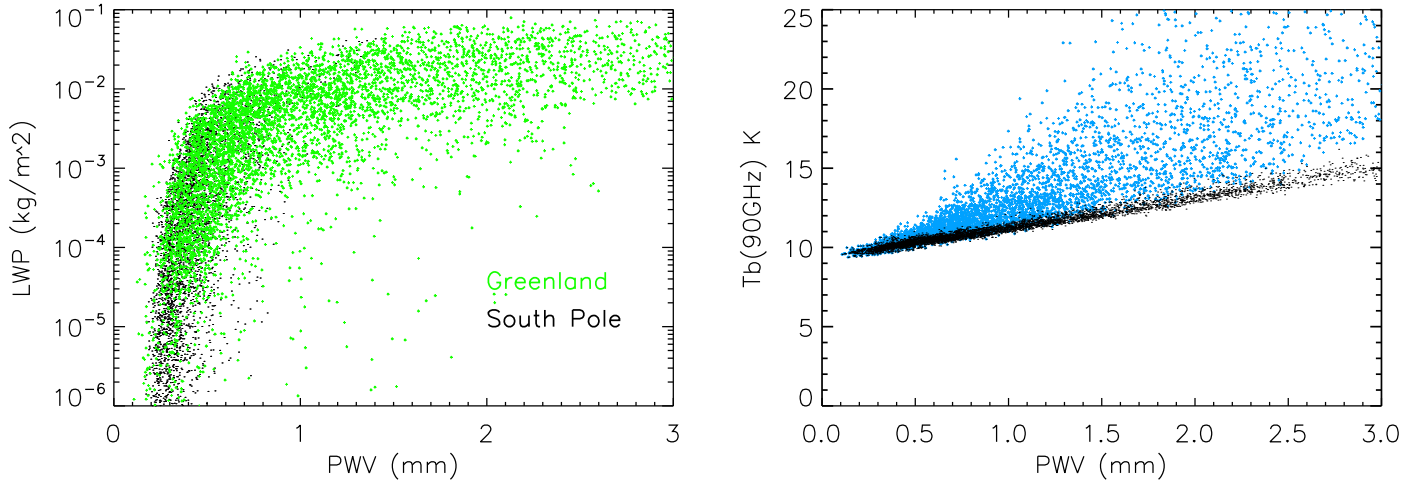

Figure 6. (Left) The liquid water path (LWP) plotted against precipitable water vapor (PWV) for the South Pole and Greenland. Liquid water starts to become an important factor when PWV $\gtrsim$ 0.5 mm. (Right) The zenith brightness temperature at 90 GHz vs. PWV at Summit Camp, Greenland. When LWP is ignored, T_b is roughly linearly proportional to the PWV (black dots). When PWV is larger, LWP adds important contributions to T_b (cyan dots). Also see Figure 4.

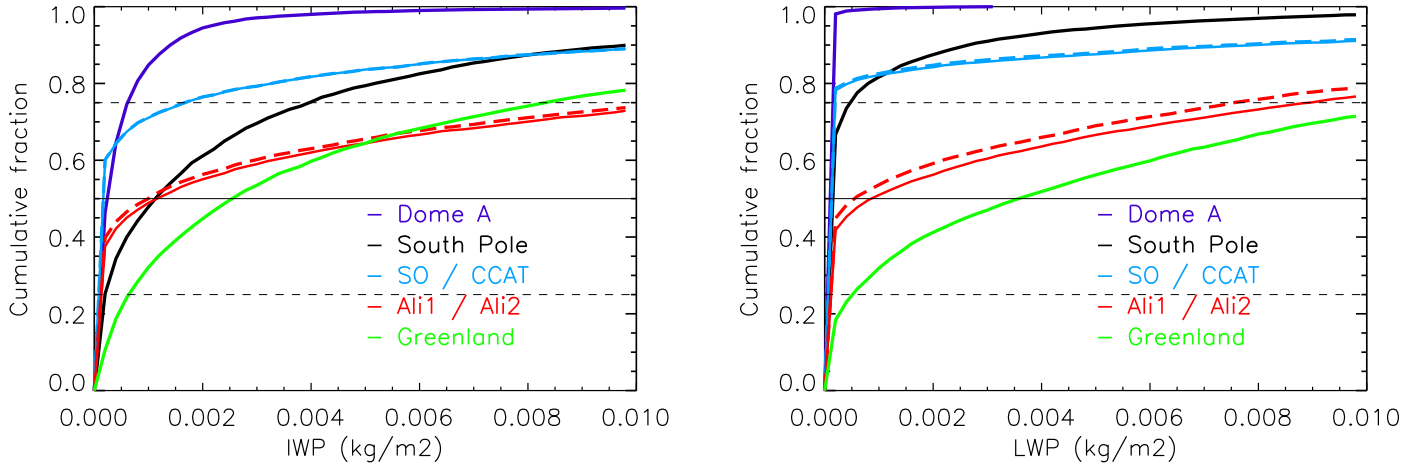

Figure 7. Cumulative distributions of IWP (left) and LWP (right) for the five sites considered in this study. As discussed in the text, liquid water clouds will have an important impact on observations.

Camp. At 90 and 150 GHz, the contribution from liquid clouds is comparable to the water vapor. Liquid affects a much smaller fraction of the data at the South Pole because the LWP median is $\sim$200$\times$ smaller. (Figure 6(a); Table 1.)

In Figure 6(b), *am* values of zenith brightness temperature at 90 GHz are plotted against PWV with (cyan) and without (black) considering the effects of liquid water. When PWV is low, sky brightness temperature is proportional to PWV. However, when PWV creeps above $\sim$0.5 mm, supercooled liquid droplets appear and become a hidden variable that adds significantly to T_b—and increase, or even dominate its fluctuations (Section 4.4).

Figure 6(b) clearly demonstrates that simultaneous measurements of PWV and LWP are necessary for a proper evaluation of the site, even though LWP is often unjustifiably omitted. Cumulative distributions of IWP and LWP are presented in Figure 7 and Table 1 for different sites. One can notice that in these data, IWP and LWP often come in at a similar level. Since ice crystals scatter less and absorb less than liquid, they do not significantly impact mm-wave observations and are listed mainly for completeness.

In Figure 8 and Table 2, zenith Planck brightness temperature T_b calculated by *am* is shown for three key CMB bands 90, 150, and 220 GHz, with and without considering the effects of IWP and LWP. Liquid water is nearly undetectable at Dome A, and only plays a minor role at the South Pole and Atacama. On the other hand, the presence of liquid water noticeably increases the sky temperature in Greenland, especially at the two lower-frequency bands important for the CMB. The level of LWP in Ali lies between Atacama and Greenland.

4.4. Brightness Temperature Fluctuations

Prior work on quantifying brightness temperature fluctuations (a.k.a. the "sky noise") for various sites often adopted specific models of atmospheric fluctuations. Estimations for the parameters in the model, such as fluctuation amplitudes or power-law index are then derived based on the observed spatial or temporal fluctuations (Lay & Halverson 2000; Bussmann et al. 2005; Sayers et al. 2010; Errard et al. 2015). The advantage of that approach is that these parameters are directly related to quantitative models. However, different papers often chose different models and used measurements made under

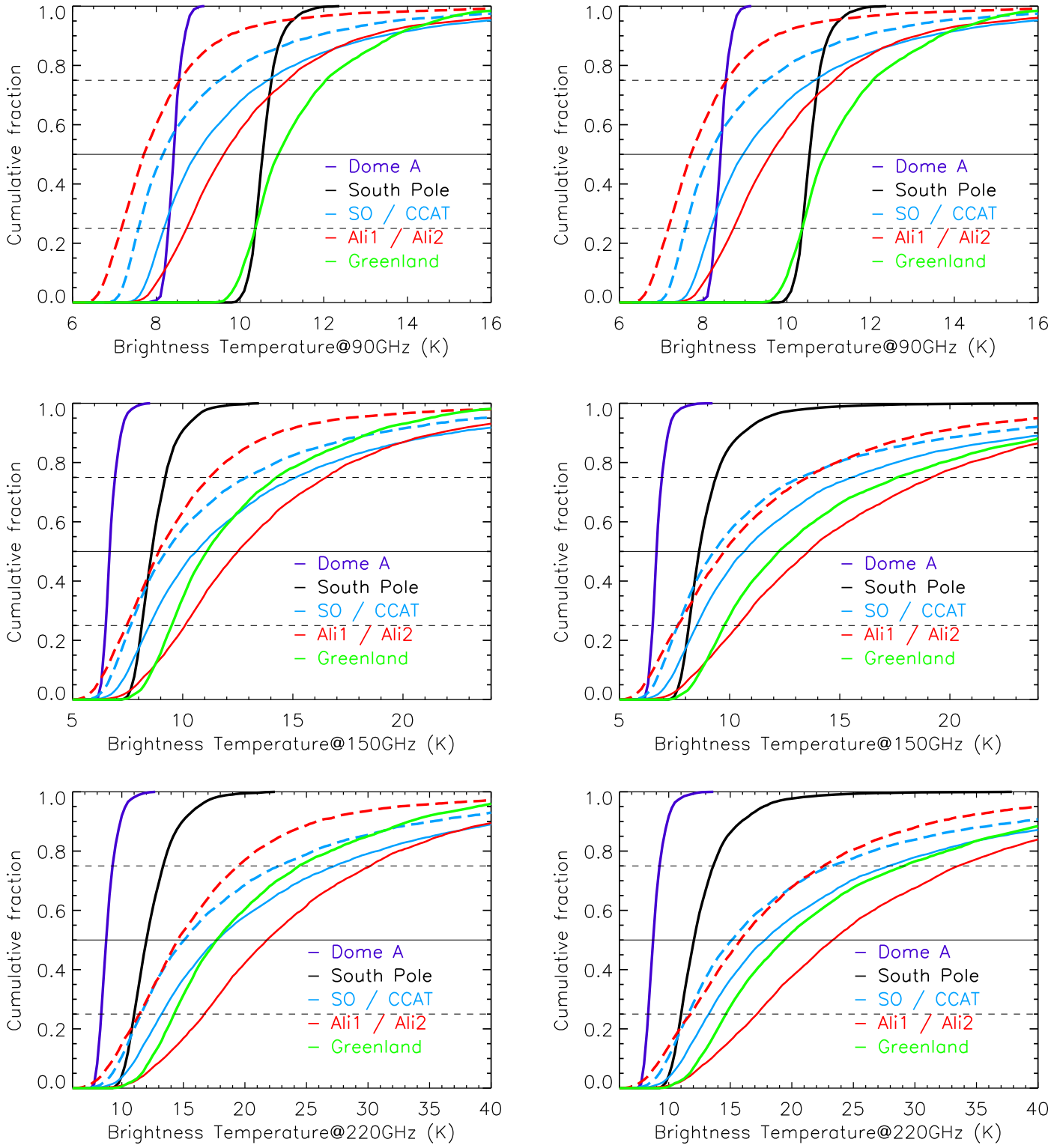

Figure 8. Zenith brightness temperature (Planck) at 90, 150, and 220 GHz calculated by the *am* radiative transfer code for the five sites considered in this paper. The calculations are repeated with (left column) and without (right column) including the effects of liquid and ice water clouds. Table 2 is the numerical summary of this Figure.

different conditions. Such variations severely complicate direct comparisons of different sites, which is a main goal of these studies. The "*d*" measures proposed in this paper based on spatial variations of specific humidity (Equation (2)) should provide simple and robust comparisons between sites. When measured in units of the South Pole *d*PWV median, the *d*PWV medians for Dome A, Greenland, Cerro Chajnantor, Simons Obs., Ali2, and Ali1 are 0.37, 4.5, 9.7, 12.4, 10.2, and 15.0, respectively (Table 1). These ratios correspond roughly to the Rayleigh–Jeans brightness temperature fluctuations ($dT_{\rm rj}$) due

Table 2
Zenith Planck Brightness Temperature T_b

		90 GHz			150 GHz			220 GHz		
		25%	50%	75%	25%	50%	75%	25%	50%	75%
Dome A	vapor only	8.29	8.42	8.53	6.50	6.69	6.93	8.33	8.73	9.25
	vp+ice+liq.	8.29	8.42	8.53	6.50	6.69	6.93	8.34	8.73	9.25
South Pole	vapor only	10.37	10.54	10.76	8.14	8.59	9.20	11.01	12.01	13.36
	vp+ice+liq.	10.37	10.56	10.84	8.14	8.62	9.37	11.01	12.05	13.61
Simons Obs.	vapor only	8.19	8.96	10.67	8.48	10.62	15.15	13.20	17.77	27.29
	vp+ice+liq.	8.19	8.98	10.90	8.50	10.67	15.57	13.22	17.85	27.97
Cerro Chaj.	vapor only	7.57	8.16	9.52	7.63	9.27	12.89	11.57	15.08	22.75
	vp+ice+liq.	7.58	8.18	9.71	7.65	9.30	13.25	11.60	15.15	23.27
Ali1	vapor only	8.72	9.61	11.15	10.09	12.50	16.53	16.70	21.81	30.19
	vp+ice+liq.	8.88	10.26	13.07	10.40	13.57	19.16	17.18	23.36	33.50
Ali2	vapor only	7.16	7.70	8.56	7.47	8.91	11.22	11.46	14.55	19.43
	vp+ice+liq.	7.27	8.18	10.17	7.65	9.75	13.56	11.78	15.83	22.57
Greenland	vapor only	10.36	10.92	12.05	9.49	11.10	14.25	14.25	17.70	24.40
	vp+ice+liq.	10.56	11.72	14.44	9.75	12.23	17.61	14.62	19.38	29.14

Table 3
PWV and LWP Fluctuations

	ΔPWV (mm)			ΔLWP (kg m^{-2})		
	25%	50%	75%	25%	50%	75%
South Pole	1.45E-03	2.76E-03	5.29E-03	…	1.00E-05	9.13E-05
Greenland	6.06E-03	1.30E-02	2.78E-02	1.33E-04	5.47E-04	1.57E-03

Table 4
Zenith (Rayleigh–Jeans) Temperature Fluctuations

			90 GHz			150 GHz			220 GHz		
			25%	50%	75%	25%	50%	75%	25%	50%	75%
Dome A	dT_{rj} (K)		5.6E-03	1.0E-02	1.9E-02	1.9E-02	3.5E-02	6.4E-02	4.2E-02	7.6E-02	0.14
South Pole	dT_{rj} (K)		1.6E-02	2.7E-02	4.9E-02	5.5E-02	9.3E-02	0.17	0.12	0.20	0.37
	ΔT_{rj} (K)	vapor only	2.24E-03	4.27E-03	8.18E-03	7.65E-03	1.46E-02	2.79E-02	1.67E-02	3.19E-02	6.11E-02
		v+liq. lnr	3.10E-03	7.08E-03	2.07E-02	9.55E-03	2.04E-02	5.08E-02	1.99E-02	4.21E-02	9.61E-02
		v+liq. quad	2.77E-03	6.18E-03	1.65E-02	8.73E-03	1.80E-02	4.13E-02	1.84E-02	3.65E-02	8.04E-02
Simons Obs.	dT_{rj} (K)		0.17	0.34	0.67	0.55	1.14	2.24	1.20	2.46	4.83
Cerro Chaj.	dT_{rj} (K)		0.13	0.26	0.54	0.43	0.89	1.80	0.93	1.91	3.89
Ali1	dT_{rj} (K)		0.25	0.41	0.69	0.82	1.38	2.31	1.78	2.98	4.98
Ali2	dT_{rj} (K)		0.16	0.28	0.50	0.52	0.94	1.66	1.13	2.03	3.59
	dT_{rj} (K)		6.39E-02	0.12	0.24	0.21	0.41	0.81	0.46	0.88	1.75
Greenland	ΔT_{rj} (K)	vapor only	9.35E-03	2.01E-02	4.28E-02	3.14E-02	6.75E-02	0.14	6.79E-02	0.15	0.31
		v+liq. lnr	3.40E-02	0.11	0.29	8.00E-02	0.21	0.50	0.14	0.36	0.81
		v+liq. quad	3.01E-02	9.41E-02	0.25	6.49E-02	0.17	0.40	0.11	0.27	0.64

to variations in water vapor (Table 4). The squares of these ratios represent the fluctuation power against which r (primordial tensor-to-scalar ratio) measurements are made.

As described in Section 2, the alternative Δ quantities have been derived from 2D data with 1 hr intervals. Table 3 shows that the median ΔPWV for Greenland is 4.7× larger than that for the South Pole. This is consistent with the factor of 4.5 quoted above for *d*PWV, giving us confidence that both measures are probing the same underlying Kolmogorov–Taylor spectra. For Summit Camp, Greenland, LWP and its fluctuations play an important role. The Δ measures of PWV and LWP provide an easy way to quantify their relative contributions to brightness temperature fluctuations. Feeding these into the *am* radiative transfer code, one can obtain approximate brightness temperature T_{rj} fluctuations, as listed in Table 4.

How ΔPWV and ΔLWP add together depends on the correlation between these quantities on relevant timescales. In Table 4, both linear (100% correlation) and quadrature sums (uncorrelated) are presented. It is noted that for Greenland, the brightness temperature fluctuations due to vapor and liquid are much larger than those from the vapor alone, even if quadrature sums are used (At 90 and 150 GHz, ΔT_{rj} is at least ∼10× larger at Summit Camp than at the South Pole).

5. Discussion

Using MERRA-2 reanalysis of atmospheric data, several remote sites have been comprehensively evaluated for mm-wave observations, with an emphasis on long integrations with high duty cycles. The numerical results have been summarized in Tables 1–4. The properties evaluated include the standard

PWV distribution, its variations (spatial and temporal) on time/angular scales relevant to future CMB observations, and the statistics of ice and liquid clouds. This work expands the scope of prior site characterization, and eliminates equipment and methodology-related uncertainties.

Dome A is confirmed to be superior to the South Pole in all measures, including PWV quartiles, sky brightness, and its fluctuations. It can be a game-changer for Galactic foreground measurements at frequencies higher than 280 GHz, which is challenging even for the South Pole.

Ali1 at 5250 m is an excellent site for the planned first-stage observations at 90/150 GHz. The PWV median and best quartile are somewhat higher than those of Atacama at the same elevation, which motivates searching for sites higher than 6000 m for high-frequency observations. Several easily accessible peaks above 6000 m between the airport and the current Ali1 site have already been identified and explored. Such high sites would have PWV quartiles and stability nearly identical to those at Cerro Chajnantor (5612 m). Plans are being made to place automatic weather stations on these candidate peaks.

Based on the distributions of PWV, Summit Camp, Greenland provides observing conditions similar to those of Cerro Chajnantor and Ali2. Perhaps the biggest surprise from the MERRA-2 reanalysis is the relative high level of liquid water clouds detected in Greenland. Not only does the LWP contribute significantly to the 90/150 GHz opacity, the sky temperature fluctuations caused by variations in LWP often dominate over those from PWV variations. This is analogous to how massive galaxies of clusters present a highly amplified version of the matter distribution of the universe. Based on MERRA-2 data, the sum effects of vapor and liquid generate brightness temperature fluctuations at a level similar to the mid-latitude sites (10× that of the South Pole). Since radiometer observing only at around the 183 GHz water line would miss the LWP and its fluctuations altogether, this result calls for simultaneous retrieval of PWV and LWP in future site surveys. It is also worth reviewing how PWVs, IWPs, and LWP are retrieved in MERRA-2 and how these quantities are correlated.

The author thanks Keiichi Asada, Nien-Ying Chou, Ken Ganga, Paul Ho, Adrian Lee, Yongping Li, Yang Liu, Shengcai Shi, Keith Thompson, Chun-Hao To, Suzanne Staggs, Wei-Hsin Sun, and Xinmin Zhang for discussions and useful suggestions to an early manuscript. The author is also thankful for the support from SCPKU (Stanford Center at Peking University), where a large part of this paper was written. Some of the analyses were done using the Goddard IDL library.

References

Abazajian, K. N., Arnold, K., Austermann, J., et al. 2015, APh, 63, 66
Bosilovich, M., Akella, S., Coyet, L., et al. 2015, NASA Tech. Rep. 2015-104606, No. 43
Bussmann, R., Holzapfel, W. L., & Kuo, C. L. 2005, ApJ, 622, 1343
Chamberlin, R. A., & Crossman, E. N. 2012, JGRD, 117, D13111
CMB-S4 Collaboration, 2016, arXiv:1610.02743
Cortes, F., Reeves, R., & Bustos, R. 2016, RaSc, 51, 1166
Errard, J., Ade, P. A. R., Akiba, Y., et al. 2015, ApJ, 809, 63
Kernasovsky, S., Ade, P. A. R., Aikin, R. W., et al. 2012, Proc. SPIE, 8452, 84521B
Lay, O. P., & Halverson, N. W. 2000, ApJ, 543, 787
Li, Y., Yang, L., Li, S., Li, H., & Zhang, X. 2017, arXiv:1709.09053
Matsushita, S., Asada, K., Martin-Cocher, P. L., et al. 2017, PASP, 129, 025001
McCarty, W., Coy, L., Gelaro, R., et al. 2016, NASA Tech. Rep. 2016-104606, No. 46
Paine, S. 2017, The am Atmospheric Model, SMA Techncical Memos 152, https://www.cfa.harvard.edu/sma/memos/
Peterson, J. B., Radford, S. J. E., Ade, P. A. R., et al. 2003, PASP, 115, 383
Radford, S. 2012, CCAT TM 112, http://wiki.astro.cornell.edu/twiki/pub/CCAT/CCAT_Memos/2012-12-21-ccat-pwv.pdf
Radford, S., & Peterson, J. B. 2016, PASP, 128, 075001
Rees, M. 1968, ApJL, 153, L1
Ricarte, A., & Dexter, J. 2015, MNRAS, 446, 1973
Sayers, J., Golwala, S. R., Ade, P. A. R., et al. 2010, ApJ, 708, 1674
Seljak, U., & Zaldarriaga, M. 1997, PhRvL, 78, 2054
Shi, S., Paine, S., Yao, Q., et al. 2016, NatAs, 1, 0001
Wu, W. L. K., Ade, P. A. R., Ahmed, Z., et al. 2016, JLTP, 184, 765
Wu, W. L. K., Errard, J., Dvorkin, C., et al. 2014, ApJ, 788, 138
Yang, H., Kulesa, C. A., Walker, C. K., et al. 2010, PASP, 122, 890
Ye, Q. Z., Su, M., Li, H., & Zhang, X. 2016, MNRAS, 457, L1